Strong sub-bandgap photoconductivity in GaP implanted with Ti

J. Olea[*, 1], A. del Prado[1], E. García-Hemme[1], R. García-Hernansanz[1], D. Montero[1], G. González-Díaz[1]

J. Gonzalo[2], J. Siegel[2]

E. López[3]

[1]Departamento de Física Aplicada III, Facultad de Ciencias Físicas, Universidad Complutense de Madrid, 28040 Madrid (Spain).

[2]Laser Processing Group, Instituto de Optica, IO-CSIC, Serrano 121, 28006 Madrid (Spain).

[3]Universidad Politécnica de Madrid, Instituto de Energía Solar, ETSI de Telecomunicación, Ciudad Universitaria s/n, 28040 Madrid (Spain).

[*]e-mail: oleaariza@fis.ucm.es

Abstract

Photovoltaic solar cells based on the intermediate band (IB) concept could greatly enhance the efficiency of future devices. We have analyzed the electrical and photoconductivity properties of GaP supersaturated with Ti in order to assess its suitability for IB solar cells. GaP:Ti was obtained by ion implantation followed by pulsed laser melting (PLM) using an ArF excimer laser. It was found that PLM energy densities between 0.35 and 0.55 J/cm^2 produced a good recovery of the crystalline structure of the GaP (both unimplanted and implanted with Ti), as evidenced by high mobility measured values (close to the reference GaP). Outside this energy density window, the PLM failed to recover the crystalline structure producing a low mobility layer that is electrically isolated from the substrate.

Spectral photoconductivity measurements were performed using the van der Pauw set up. For GaP:Ti a significant enhancement of the conductivity was observed when illuminating the sample with photon energies below 2.26 eV, suggesting that this photoconductivity is related to the presence of Ti in a concentration high enough to form an IB within the GaP bandgap. The position of the IB was estimated to be around 1.1 eV from the conduction band or the valence band of GaP, which would lead to maximum theoretical efficiencies of 25% - 35% for a selective absorption coefficients scenario and higher for an overlapping scenario.

Introduction

Photovoltaic devices fabricated with intermediate band (IB) semiconductors have the potential of greatly exceed the Shockley-Queisser efficiency limit [1, 2]. While silicon solar cells have the advantages of low cost raw material and very mature technology, a semiconductor with a bandgap close to 2 eV would theoretically attain the optimum efficiency in an IB solar cell, reaching values over 60% under concentrated light. Gallium phosphide, with a 2.26 eV bandgap could be an interesting candidate for this task. As a reference, the maximum efficiency of an ideal GaP solar cell without IB and without concentration would be around 20% [3]. However, practical GaP devices only achieve efficiencies below 5% because they are limited by low diffusion lengths and high surface recombination velocities [4, 5].

Theoretical studies claim that the introduction of several different impurities in GaP could form an IB [6, 7]. Among other transition metals, Ti has been theoretically analyzed and seems to be the most promising element [8, 9]. The position of the IB inside the GaP bandgap would be of special importance for the estimation of the efficiency limit of the GaP:Ti system. Although we could not find any clarifying study regarding the position of Ti deep levels in GaP, some evidences point to values located at 0.66 eV and 0.96 eV [10, 11]. Regarding theoretical calculations for IB GaP:Ti, the feasibility of the material seems to be demonstrated [12-15], but its location inside the bandgap has not been fully predicted yet. Moreover, most methods do not take into account indirect transitions and therefore the indirect bandgap of GaP cannot be correctly calculated.

One of the possibilities to form an IB in GaP out of the Ti deep levels is the introduction of a high concentration of Ti in the GaP lattice to induce a transition from non-radiative recombination to radiative recombination [16]. We will name the required concentration as Luque's. Since the solid solubility of deep levels is usually much lower than Luque's limit, obtaining the IB can be a challenging task. In general, solid solubility of deep levels in III-V semiconductors is around 10^{17} cm^{-3} [11], while Luque's limit would be around 10^{20} cm^{-3} [16]. Therefore, techniques working out of thermodynamical equilibrium should be used to achieve the required impurity concentration. For other IB materials based on III-V semiconductors, such as highly mismatched alloys, the combination of ion implantation and pulsed-laser melting (PLM) has been successfully carried out [17-19]. The PLM can melt and recrystallize the implanted layer, trapping most of the implanted impurities while resulting in a high crystal quality with impurity concentration well beyond the solid solubility limit. Laser processes for semiconductors were deeply studied in the 70 – 80's [20], but since then, most of the research related to III-V semiconductors has been conducted with GaAs.

In Refs. [21, 22], we concluded that melting and recrystallization processes under excimer laser radiation are not straightforward for GaP. It seems that for high recrystallization velocities GaP is not able to regrow following the crystal structure of the underlying non-melted substrate, and polycrystalline phases appear, though for high energy densities the crystal quality and the size of the grains increased. Recent results [23] seem to indicate that high quality recrystallization takes place just only in a quite narrow laser energy density window. This is similar to previous results for GaAs laser annealing [24, 25] and suggest a quite different scenario compared to the much more straightforward recrystallization by laser

processing of Si [26]. Besides, Ti implanted GaP at high doses has been studied in [27] in the scope of IB materials, concluding that the material can be fabricated with high crystal quality using electron-beam pulse annealing. However, no electronic or optoelectronic properties of Ti supersaturated GaP have been reported yet.

In this work we first find a suitable process window for excimer laser recrystallization of Ti implanted GaP using a specific PLM system. To analyze the quality of the processed films we show the measured electronic transport properties as a function of temperature. Afterwards we present the spectral sheet photoconductance of several GaP samples implanted with Ti and well recrystallized and discuss the results.

Experimental

Undoped GaP grown by the Czochralski method in the <100> direction, single side polished, 500 μm of thickness, with a resistivity around 0.3 Ωcm at room temperature (carrier concentration in the 2×10^{16} – 8×10^{16} cm^{-3} range), was implanted in a refurbished VARIAN CF3000 Ion Implanter by the polished surface with two $^{48}Ti^{+}$ doses, 8×10^{14} cm^{-2} and 2×10^{15} cm^{-2}, at energies of 28 keV and 32 keV, respectively. All implantations were conducted using a 7° tilt angle. For these implantation parameters, Stopping and Range of Ions in Matter (SRIM) simulations yielded projected ranges of 23 and 26 nm, and a peak Ti concentrations of 2.57×10^{20} cm^{-3} and 5.87×10^{20} cm^{-3}.

To recover the lattice damaged during the implantation process, a subsequent PLM process was performed in air. Implanted samples were irradiated with an ArF excimer laser (λ=193 nm, 20 ns full width half maximum). An imaging set up was used in order to have a top-hat laser beam profile at the irradiation plane. This consisted of a fused silica planoconvex lens (focal length 41 mm at 193 nm) that precisely imaged a 3 x 3 mm^2 aperture, inserted into the central region of the laser beam path, 53 cm after the laser output, onto the sample surface to lead to a **0.95 ± 0.02 x 0.95 ± 0.02 mm^2** beam size at the irradiation plane. Thus, the laser beam was tiled across the surface of the samples to process their whole area using a single laser pulse in each step. The overlapping between consecutive horizontal and vertical irradiated areas was 5 μm and 10 μm, respectively. To find the best quality recrystallization window of the PLM for unimplanted GaP, a set of samples was fabricated and the energy density of the ArF excimer laser pulse was swept in the 0.3 – 0.55 J/cm^2 range. The energy density uncertainty was estimated to be ~5%. These values were chosen because they are known to produce good quality recrystallization on other III-V semiconductors for a similar excimer laser wavelength [23]. Regarding the lower limit, an energy density over 0.3 J/cm^2 is needed to homogeneously melt the surface of GaAs [28].

After the PLM processes, in order to measure the electronic transport properties and the spectral sheet photoconductance, samples were cut in 0.5×0.5 cm^2 square pieces and contacted on the corners of the implanted surface to use the van der Pauw set up. To fabricate the contacts, four triangular masks were used to deposit 50 nm of Ni by e-beam evaporation followed by a Joule evaporation of 200 nm of Au/Ge (88:12). Both evaporations were performed without breaking the vacuum. To improve the contact quality for the non-

implanted samples a rapid thermal annealing (RTA) at 500 °C during 30 s in Ar atmosphere was conducted. No RTA was performed on the implanted samples since they contain a very high Ti concentration. This concentration might be over the solid solubility limit and therefore could be in a metastable situation that could be modified by the RTA process. This supersaturation is the key of many of the impurity band materials [29, 30]. Nevertheless, the high concentration of Ti would assure a good contact characteristic for the van der Pauw set up.

Sheet resistance and Hall effect measurements were performed at variable temperature in the 75 – 300 K range in a closed-cycle Janis cryostat. A Keithley 4200 SCS with four source and measure units was used, and the van der Pauw configuration was switched, changing also the current source (1 mA) and magnetic field (0.89 T) directions to measure and average a total of 8 configurations for the sheet resistance and 16 configurations for the Hall effect. From these measurements the Hall mobility was also obtained.

Time-of-Flight secondary ion mass spectrometry characterization was conducted on implanted samples to obtain the Ti concentration as a function of depth. A TOF-SIMS^5 fabricated by ION-TOF with a Bi_3^+ (0.25 pA) primary gun at 25 kV was used, extracting at 10.5 kV. For the sputtering an O_2 gun was configured at 1 kV producing a 300×300 μm^2 crater. Some Ti as-implanted samples without subsequent thermal process were used for calibration purposes, using the implanting dose as a reference. To convert from sputter time to depth, the final crater was characterized by contact with a Sloan Dektak profilometer and a constant erosion rate was assumed.

The room temperature spectral sheet photoconductance of the samples was measured using the van der Pauw configuration to reduce the effect of the series resistance of the contacts. Measurements were conducted with a current source of 1 mA and illuminating by the implanted surface in the 250 – 1125 nm range with a Horiba iHR320 spectrophotometer with two diffraction gratings. The light source was a 250 W tungsten halogen lamp and slits were configured for different measurements at 0.5 mm and 2 mm, producing a resolution of 1.16 and 4.62 nm, respectively. Long-pass filters were placed at 320, 550 and 750 nm. Light was mechanically chopped at 23 Hz and the AC van der Pauw voltage was measured with a Stanford Research System SR830 DSP lock-in amplifier in (A-B) configuration. To calibrate the light source in terms of W/cm^2 a calibrated Si S2281 photodiode (Hamamatsu) in photovoltaic mode was used. To guarantee the reliability of the results, the spectral sheet photoconductance measurements were repeated and confirmed using a 100 W tungsten halogen lamp and a NewPort Cornerstone 7400 monochromator. **Finally, to measure the spectral sheet photoconductance in the short and mid infrared (1 – 5 μm) range we used a TMc300 Bentham monochromator with a 140 W Globar (SiC) source. The intensity of the light was calibrated with a Bentham pyrometric detector.**

Detailed Balance

The efficiency limit of IB solar cells based on GaP was obtained by means of the detailed balance model used in [1]. This model assumes that: (1) carriers recombine only by means of radiative processes; (2) the sun and the surroundings of the solar cells are black

bodies at temperatures 6000 K and 300 K respectively, and the IB solar cells are bodies at 300 K; (3) the IB is a zero width energy band; (4) all photons with energy higher than the lowest sub-bandgap are absorbed; (5) the absorption coefficients related to the optical transitions are selective; (6) photons emitted by the solar cells can be reabsorbed by means of photon recycling; (7) the carrier mobility in the CB and the VB is infinite (or what it is the same, the quasi-Fermi levels are constant); (8) a perfect mirror is located at the back of the solar cell.

In Fig. 1.a we present the efficiency limit of ideal IB solar cells based on GaP under maximum sunlight concentration (46050 suns). In this plot the x-axis represents the IB position with respect to the conduction band (CB) or the valence band (VB). Due to the symmetry of the calculations, above 1.1 eV a mirrored curve would exist with the complementary position of the IB. Also, we show as references the maximum efficiency achievable for a GaP single bandgap solar cell (bandgap of 2.26 eV) under maximum concentration (calculated in this work) and the maximum efficiency achievable for an ideal IB solar cell [1]. A band diagram is shown in Fig. 1.b depicting the IB energy versus the CB energy, i.e. E_{CB}-E_{IB}.

As it can be seen, the calculated efficiencies are well above the efficiency of a single bandgap solar cell, and for E_{CB}-E_{IB} = 0.85 eV (or E_{IB}-E_{VB} = 0.85 eV) the efficiency is close to the IB optimum. These theoretical results would validate GaP as an interesting material for IB research. Since actual GaP solar cells have maximum efficiencies below 5% [4] there is much room for improvement.

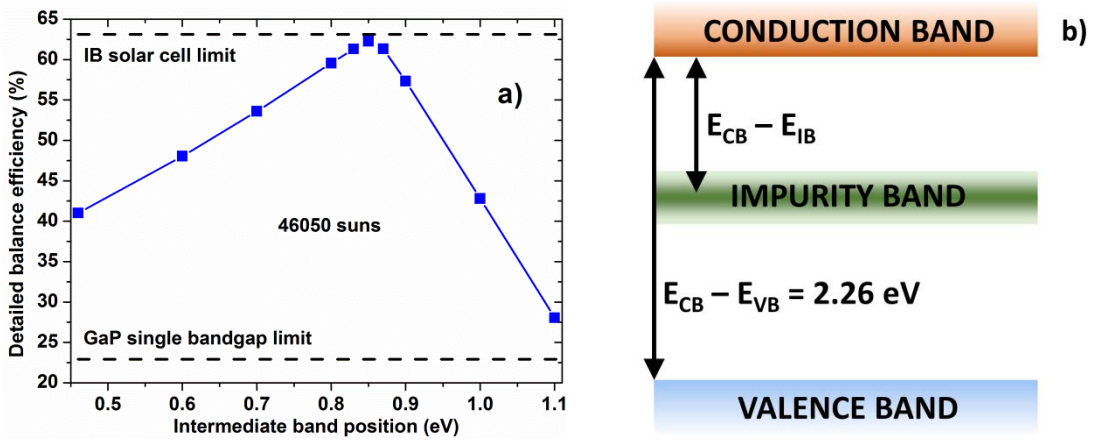

Figure 1. a) Detailed balance results for a 2.26 eV bandgap solar cell with an IB. Results are plotted as a function of the position of the IB. Calculated efficiency overcomes the one of a single bandgap solar cell, and for E_{CB}-E_{IB} = 0.85 eV (or E_{IB}-E_{VB} = 0.85 eV) is close to the IB ideal limit. **a)** Band diagram of an IB semiconductor based on GaP.

Results

Fig. 2 shows the room temperature values of sheet resistance (a) and Hall mobility (b) of different unimplanted GaP samples as a function of the energy density of the PLM. Results are shown together with previous results from a study performed by some of the authors using a KrF (λ=248 nm) excimer laser [22] with a 20 ns pulse to process unimplanted GaP. The effect of the different laser wavelengths (ArF, 193 nm, in this study; and KrF, 248 nm, in [22])

should be negligible, since the absorption length would be between 5 and 10 nm in both cases and the pulse time is the same.

As it can be seen in Fig. 2.a, after the PLM the sheet resistance of the samples approaches the sheet resistance of the reference substrate (not laser processed) only for a narrow range of energy densities. Outside this range the sheet resistance of the samples greatly increases. A similar trend occurs for the Hall mobility: in the same energy density range the mobility of the processed samples is similarly high to the mobility of an unprocessed reference. Outside this range the mobility has lower values and for the highest energy densities the Hall mobility has a negligible magnitude.

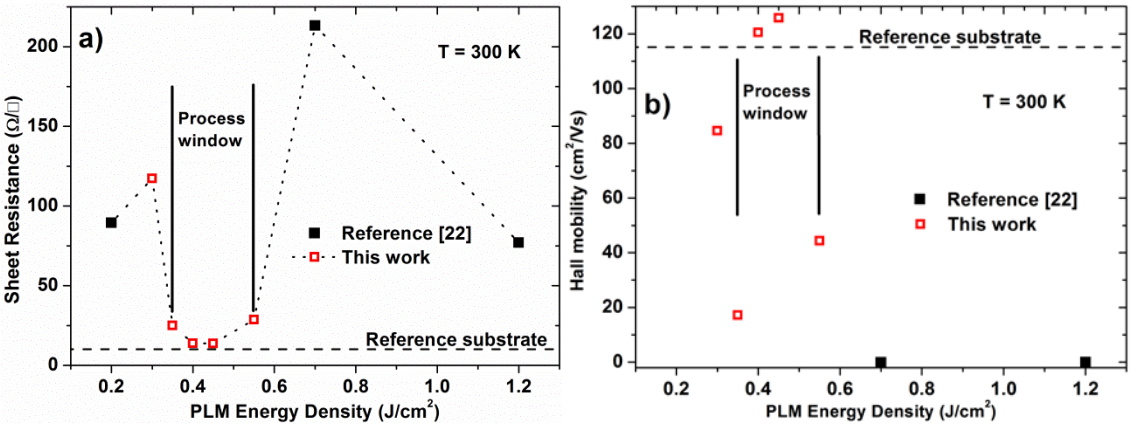

Figure 2. a) Room temperature sheet resistance of PLM processed unimplanted GaP samples as a function of the excimer laser energy density. In the 0.35 – 0.55 J/cm^2 range the resulting sheet resistance is almost equal to the sheet resistance of untreated GaP. Outside this range the sheet resistance increases abruptly. **b)** Room temperature Hall mobility of PLM processed unimplanted GaP samples as a function of the excimer laser energy density. In the 0.35 – 0.55 J/cm^2 range the resulting mobility is almost equal to (even higher than) the sheet resistance of untreated GaP. Outside this range the mobility decreases abruptly. Horizontal dashed lines in a) and b) correspond to the sheet resistance and Hall mobility of untreated GaP.

To deeply analyze the effect of the energy density of the PLM on the electronic transport properties of GaP, we compare in Fig. 3, as a function of the measured temperature, the sheet resistance (a) and Hall mobility (b) values of an untreated GaP reference sample, an unimplanted GaP sample PLM processed at 0.4 J/cm^2 (inside the process window shown in Fig. 2), an unimplanted GaP sample PLM processed at 1.2 J/cm^2 (outside the process window) and a Ti implanted (2×10^{15} cm^{-2} dose) GaP sample subsequently PLM processed at 0.52 J/cm^2 (also inside the process window). At temperatures over 100 K optical phonon scattering processes dominate producing mobility with an almost potential trend [31]. Except in the case of the undoped GaP samples processed at 1.2 J/cm^2 and thus, outside the process window, high mobility values around 100 cm^2/Vs at room temperature are obtained. These values are consistent with the electron concentration measured (10^{16} – 10^{17} cm^{-3}), pointing to a high crystal quality [31]. Even with the high Ti dose implanted, the GaP:Ti sample presents electronic properties almost equal to the reference substrate. Regarding the sample processed at 1.2 J/cm^2, the behavior of both the mobility and the sheet resistance are completely different from the other samples. This sample presents negligible values for the mobility and an almost constant sheet resistance.

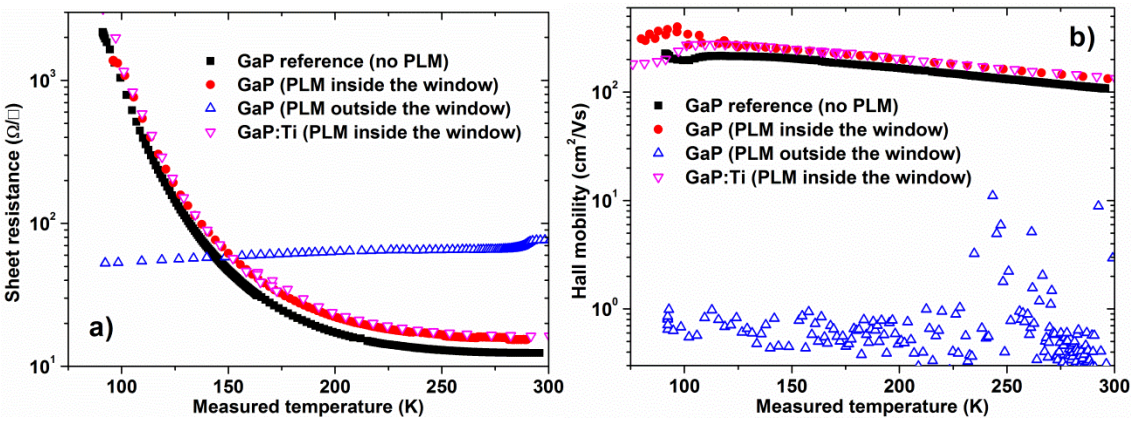

Figure 3. a) Sheet resistance of GaP samples as a function of the measured temperature. The figure includes an untreated GaP reference sample, an unimplanted GaP sample PLM processed at 0.4 J/cm^2 (inside the process window shown in Fig. 2), an unimplanted GaP samples PLM processed at 1.2 J/cm^2 (outside the process window) and a Ti implanted (2×10^{15} cm^{-2} dose) GaP sample subsequently PLM processed at 0.52 J/cm^2 (also inside the process window). **b)** Hall mobility as a function of the measured temperature of the same samples presented in a).

To analyze the Ti concentration in the implanted layer, Fig. 4 shows the ToF-SIMS results of two implanted samples that will be studied below. The concentration is extremely high in both samples, overcoming the Luque's limit in a surface layer of about 30 nm and 55 nm, respectively.

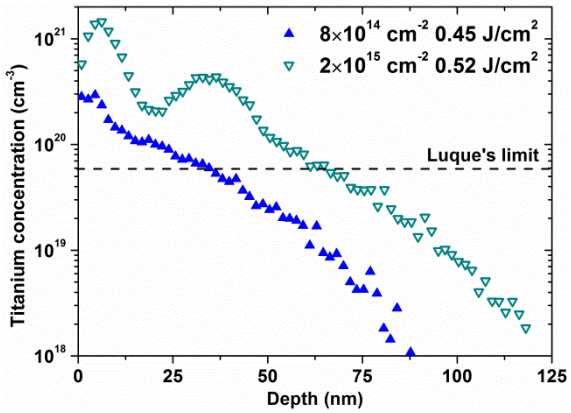

Figure 4. Titanium concentration as a function of depth, obtained by ToF-SIMS measurements, of two GaP samples implanted with 8×10^{14} cm^{-2} and 2×10^{15} cm^{-2} Ti doses, and PLM processed with an energy density of 0.45 J/cm^2 and 0.52 J/cm^2, respectively.

Representative results for several GaP samples of the spectral response measurements as a function of the photon wavelength are shown in Fig. 5.a, while Fig. 5.b shows a sketch of the experimental set-up. We present the spectral sheet photoconductance of a GaP reference unimplanted sample, of a GaP unimplanted sample PLM processed and of two Ti implanted GaP samples PLM processed after the ion implantation. **The Ti implanted samples are the same ones analyzed by ToF-SIMS in the previous figure.** For all the samples shown in Fig. 5.a, the PLM processes were conducted at energy densities inside the 0.35 – 0.55 J/cm^2 range.

Regarding the shape of the spectral sheet photoconductance curves, all the samples show the onset of the indirect bandgap of GaP at about 2.26 eV (λ≈550 nm) [32]. The GaP direct bandgap at about 2.78 eV (λ≈450 nm) [33] is also evident for all the samples except the one without laser process. Both unimplanted samples reach the noise level at about 550 nm.

However, a below bandgap response is measured for the Ti implanted samples, with a measurable signal up to 850 nm and 1000 nm. **Over 1000 nm no signal was measured for any of the samples, not even with the dedicated infrared monochromator. Finally, a**n abrupt minimum around 550 nm is present in the Ti implanted samples. This feature has been measured with reliability and appears in all the samples implanted with Ti. A phase change of about 40° is also measured by the lock-in at about 550 nm for the Ti implanted samples (see Supplementary information section).

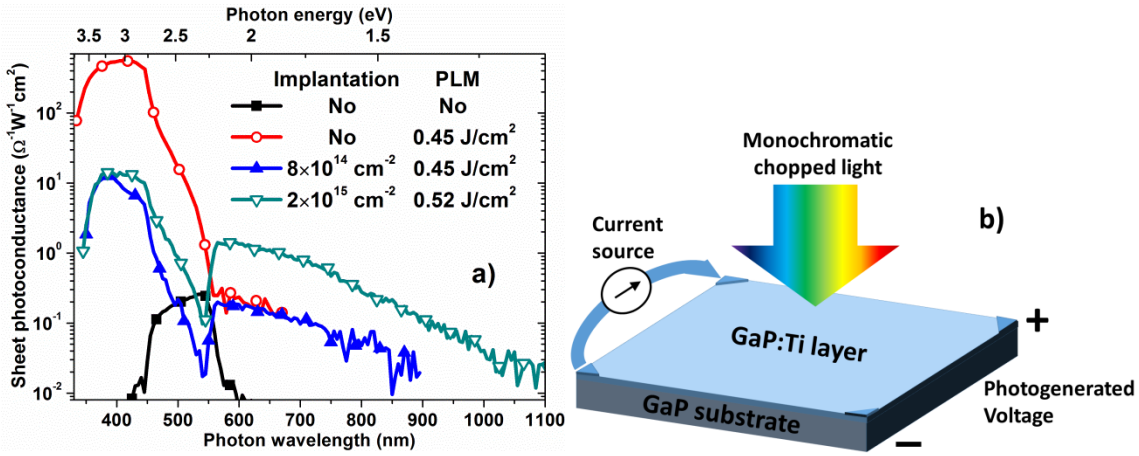

Figure 5. a) Spectral sheet photoconductance of several GaP samples as a function of the photon wavelength. This magnitude has been calibrated with the incident light power density. Results are presented for two unimplanted GaP samples, with and without PLM, and for two Ti implanted samples (doses: 8×10^{14} cm^{-2} and 2×10^{15} cm^{-2}) PLM processed. All PLM processes were conducted at energy densities inside the process window depicted in Fig. 2. For the unimplanted and PLM processed sample (red-circles), the measured signal at wavelengths over 550 nm is just "calibrated" noise, and no useful voltage could be obtained in this range. The uncalibrated data can be shown in the "Supplementary information" section. **b)** van der Pauw set-up for the measurement of the spectral sheet photoconductance.

Discussion

The results presented in [22] showed that when GaP recrystallization was not good the Hall effect measurements resulted in negligible mobility values, as shown for the sample processed at 1.2 J/cm^2 (Fig. 3b). As a consequence of this negligible mobility, outside the 0.35 – 0.55 J/cm^2 range there is an abrupt increase of the sheet resistance (Fig. 2.a). The high values of the sheet resistance point to a blocking mechanism between the PLM processed layer and the untreated substrate, since a parallel conduction would result in a sheet resistance lower than any of the layers (shown also in Fig. 3.a). This mechanism that blocks transversal conduction may be related to the formation of a potential barrier between the crystalline GaP substrate and the poorly crystallized surface layer after PLM [34]. This potential barrier would be produced by the interface defects.

For a good recrystallization of the GaP surface we suggest that the energy density of the laser process has to be restricted to a very narrow process window. This conclusion is consistent with Yuan et al. [23] results, who recently showed by means of Rutherford backscattering and TEM measurements that the optimal energy density of the laser process to

recrystallize GaP implanted samples would be around 0.4 J/cm^2 for a laser system similar to the one used in this work. In our measurements the process window would be delimited by the abrupt decrease of the Hall mobility (the 0.35 – 0.55 J/cm^2 range), which has been proved to be very sensitive to the recrystallization process. Taking into account this sensitivity, we consider that a high measured mobility for samples PLM treated with energy densities inside the process window is a fingerprint of a layer recrystallized with high quality. A similar process window has been reported for other III-V semiconductors [24, 25] yet other materials, such as silicon [35], are characterized by a much broader process window, therefore being more easily recrystallized by a laser process.

Due to the similarity of the electronic transport properties of three of the samples presented in Fig. 3 we suggest that these properties would account for parallel conduction by the surface processed layer and the substrate. The slight variations shown for these three samples would be originated by differences in the wafer batch, and fit within the range measured by the supplier. These effective properties would be highly influenced by the substrate properties, since the substrate is more than three orders of magnitude thicker than the surface PLM processed layer and has high crystal quality and therefore high mobility. The high carrier concentration in the substrate would also make this part of the sample to dominate in conduction. **Even with the extremely high Ti concentration present in the implanted samples (see Fig. 4) the effective electronic transport properties are almost equal to the reference substrate ones in all the temperature range measured. This would point that the Ti impurities are not significantly contributing to conduction in the GaP:Ti samples. To confirm this hypothesis, future research with samples based on semi-insulating GaP is now under way to measure the properties of the GaP:Ti material without any interference of the substrate.** On the contrary, the sample processed at 1.2 J/cm^2 (outside the process window) shows a negligible mobility (Fig. 3.b). It seems again that for laser processes carried out with energy density outside the process window the substrate is no longer present in the measurement, as a consequence of a deficient recovery of the crystalline quality, and we only obtain the properties of the defective processed layer [22].

It is also interesting to remark that the Ti implanted GaP sample has mobility values (Fig. 3.b) that point to a good recrystallization of the implanted layer. This would mean that for the Ti implanted doses used in this work the laser process window would remain in the same energy density range. It is important to recall that the Ti doses used are extremely high, resulting in Ti concentrations peaking above 10^{20} cm^{-3}, which are in principle in the range needed for the IB formation [16].

Therefore, the above presented results demonstrate that it is possible to achieve high quality recrystallization of unimplanted and Ti implanted GaP layers within a narrow PLM process window. We can now analyze the effect of PLM on the spectral response of the samples (Fig. 5.a). Firstly we should compare the sheet photoconductance of the two unimplanted samples. The shapes of the curves are quite different, having the PLM processed sample a much stronger response. Both curves show an onset at about 550 nm, i.e. the indirect bandgap of GaP, but only the PLM processed sample shows another increase for the direct bandgap of GaP (around 450 nm). Below 400 nm the PLM processed sample presents a decay that is usually attributed to surface recombination [4, 36]. In the case of the

unimplanted sample without PLM, a similar decay is produced, but in this case at wavelengths below 500 nm. We suggest that surface recombination is much stronger in the second case and therefore the effect takes place at higher wavelengths. Similarly, in [36] authors show how the quantum efficiency of GaP solar cells can be enhanced in the short-wavelength region by reducing the surface recombination velocity and increasing the lifetime in the surface layer (emitter). The PLM might have passivated in some way the surface, reducing recombination and increasing the sheet photoconductance.

The exact origin of this possible surface passivation is unknown at the present moment, and more research is taking place to elucidate it. It is important to note that all samples PLM processed with energy densities inside the laser process window shown in Fig. 2 have a sheet photoconductance spectrum much higher than the one of the untreated GaP reference sample and with a shape similar to the one of the unimplanted and PLM processed sample at wavelengths below 550 nm. This fact would point to the PLM as the cause for the possible passivation. Since PLM is conducted in air, the passivation might have occurred due to an oxidation process. This hypothesis is consistent with the fact that the PLM would only modify a surface layer of about 100 nm, since the 193 nm light of the ArF laser is absorbed superficially [37]. Therefore these differences cannot be originated in the bulk, leading again to a surface effect. In the case of other III-V semiconductors, such as GaAs, laser processing in air can produce a time-stable surface passivation [38]. A GaAs surface cleaning by removing a low quality native oxide, followed by S passivation, by means of excimer laser irradiation has been also reported, showing in some cases an increase of the photoluminescence intensity [39, 40].

For wavelengths above 550 nm (energies below the indirect GaP bandgap), no sheet photoconductance is observed for the unimplanted samples. On the other hand, a new photoconductance mechanism appears for the Ti implanted samples in this sub bandgap region. We suggest that its origin is related to the high Ti concentration introduced. The **Ti concentration is high enough to overcome the Luque's limit (see Fig. 4), and therefore an IB might have formed due to overlapping of the Ti deep levels in the implanted GaP:Ti layer** [16]. This IB material could take advantage of a broader part of the solar spectrum and in principle become the core of a more efficient GaP solar cell.

A minimum of the sheet photoconductance is observed in the spectra of the Ti implanted samples at about 550 nm (Fig. 5.a). This feature is very abrupt and interestingly it is located close to the energy of the indirect bandgap of GaP. This kind of feature has been previously reported [41-43] but it is particularly remarkable in our spectra. At wavelengths below 550 nm the trend is similar to the one of the PLM processed unimplanted GaP sample, showing the sheet photoconductance related to the bare GaP bandgaps transitions. Special care was taken in the measurement of this feature, avoiding any misinterpretation of the results originated in the experimental system. In fact, the samples were measured in two different systems, confirming the results. Moreover, the fact that the reference samples do not present this feature indicates that it is not an artifact of the measurement. The 40° phase difference measured above and below 550 nm would neglect the hypotheses of having negative photoconductivity or two competing processes with opposite current directions (i.e. photoconductive and photovoltaic processes), since this would produce a 180° phase difference. It has been reported that IB materials can have an abrupt decrease of the

absorption coefficient related to the transitions involving the IB [14, 15]. At certain energies the probability of a transition can decrease due to the specific distribution of the density of states of the three bands. This hypothesis to explain the appearance of this abrupt dip in the spectral sheet photoconductance spectra would be in agreement with reference [43].

To get insight on the new transitions related to Ti, sheet photoconductance curves in Fig. 5.a were fitted to Eq. (1). Our hypothesis is that the sheet photoconductance would be proportional to the absorption coefficient at energies close to the bandgap, and therefore the bandgap values could be extracted in this way [44]:

$$\Delta G_s h\nu = A\left(h\nu - E_g\right)^n \qquad (1)$$

where ΔG_s is the sheet photoconductance, $h\nu$ is the photon energy to normalize for the number of incident photons, A is a constant, and n would take the value 0.5 for direct transitions and 2 for indirect transitions.

Eq. (1) fittings for the GaP sample implanted with the 2×10^{15} cm^{-2} Ti dose and PLM processed with 0.52 J/cm^2 are shown in Fig. 6.a. For the transitions at about 2.78 eV we used the direct bandgap approximation, and the indirect bandgap approximation was used for the other two transitions. In particular, for the transition below 2.26 eV, i.e. the new transition related to Ti, the indirect approximation could be fitted better and in a wider range in comparison to the direct bandgap approximation.

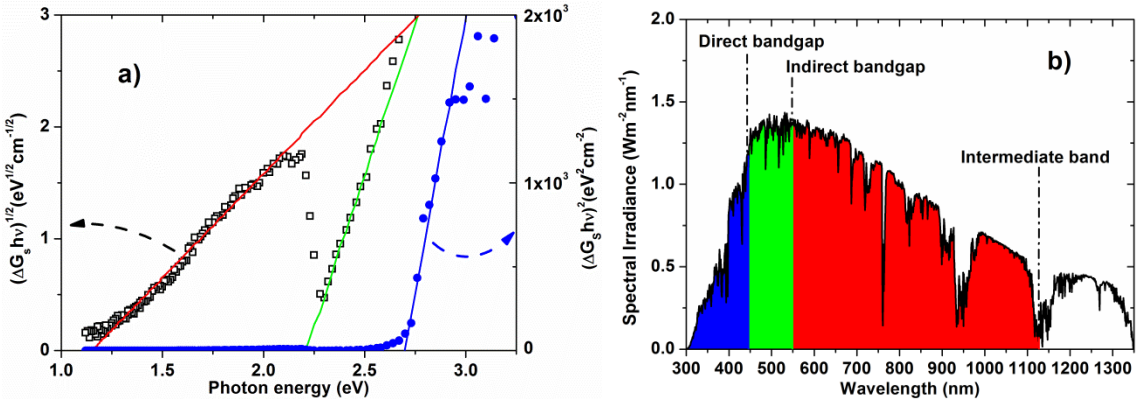

Figure 6. a) Fittings of the spectral sheet photoconductance data to Eq. 1 for the different transitions observed in Fig. 5.a for the sample implanted with the 2×10^{15} cm^{-2} Ti dose and PLM processed with 0.52 J/cm^2. The direct transition fitting corresponds to the right axis while the indirect transitions correspond to the left axis. **b)** Solar spectral irradiance as a function of the wavelength. The transitions values obtained from the fittings shown in Fig. 6.a are indicated. A pure GaP solar cell would absorb at wavelengths below 550 nm (indirect bandgap in green and direct bandgap in blue) while a solar cell including GaP:Ti could also take advantage of the 550 – 1100 nm range (red).

Fitted values for all the transitions of all the samples shown in Fig. 5.a are presented in Table 1 (the fitted curves can be seen in the Supplementary information section). As it can be seen, the values of both the indirect and the direct bandgaps of GaP, ideally located at 2.26 eV and 2.78 eV at room temperature are well measured, being the highest deviation of about 0.1 eV, i.e. less than 5%. The error in the direct bandgap analysis is higher than the one of the indirect bandgap since in the first case the wavelength range for the fitting is lower and, moreover, the indirect transition overlaps with the direct one. This good agreement would

validate the above stated assumption of the proportionality between the sheet photoconductance and the absorption coefficient at energies close to the bandgap. However, in the case of the unimplanted and non PLM processed sample the direct bandgap value could not be extracted. The bandgap value of this sample has also the highest error due to the low signal intensity of the voltage obtained from the spectral sheet photoconductance measurement.

Ti Dose	PLM	Indirect	Direct	Indirect
0	No	2.16 eV		
0	Yes	2.20 eV	2.70 eV	
8×10^{14} cm^{-2}	Yes	2.22 eV	2.70 eV	1.06 eV
2×10^{15} cm^{-2}	Yes	2.21 eV	2.69 eV	1.15 eV

Table 1. Fitted values to Eq. 1 for the transitions shown in the sheet photoconductance spectra for all the samples presented in Fig. 5.a. Both the energy values of the indirect and the direct bandgap of GaP are well measured. The new transition related to the IB formed by the Ti levels is fitted at about 1.1 eV.

Regarding the values extracted from the Eq. 1 analysis for the Ti implanted samples, we suggest that the sheet photoconductance at wavelengths over 550 nm is originated from indirect transitions involving the new IB located at about 1.1 eV (about 1100 nm) from the VB or CB of GaP. This band would be formed by the delocalization of Ti deep levels due to the high impurity concentration [16]. This value is just close to the middle of the 2.26 eV bandgap and would make GaP:Ti sensible to the 550 – 1100 nm range (notice the red range in Fig. 6.b). Relating the values of the new band transitions shown in Table 1 with the results presented in Fig. 1.a, we conclude that with the Ti doses used in this study the maximum achievable efficiency for a GaP:Ti solar cell would be around 25% - 35%. These values would be higher than the efficiency for a single bandgap GaP solar cell, but close to the Si Shockley-Queisser limit (around 30%).

The analysis shown in Fig. 1.a was performed assuming that the absorption coefficients of the different transitions would not overlap, i.e. they are selective. It has been reported that for the case in which the IB is located close to the middle of the bandgap of the semiconductor, an overlapping scenario would be theoretically more efficient [45]. Also, it seems that we could attempt to optimize the IB position by varying the fabrication parameters, specifically the implantation dose [8]. Finally, these results open the possibility of implanting other transition metals, such as V, Cr or Sc, which have been theoretically proposed to form an IB in GaP [7].

Conclusions

GaP supersaturated with Ti was obtained by means of ion implantation followed by PLM. The energy density of the PLM was found to be critical to achieve a good crystallinity recovery after the ion implantation. A narrow energy process window between 0.35 and 0.55 J/cm^2 was determined for an adequate crystalline structure for both unimplanted samples and samples implanted with Ti.

A significant photoconductivity signal was measured for the Ti implanted samples for energies below the bandgap of GaP, which we attributed to the presence of Ti in a sufficient concentration to form an IB within the GaP bandgap. The position of this IB was estimated to be close to the midgap, around 1.1 eV from the CB or the VB. From a detailed balance analysis, this would lead to a maximum efficiency in the 25% - 35% range assuming that both transitions involving the IB (from VB to IB and from IB to CB) do not overlap. Higher efficiency is expected in an overlapping absorption scenario. These results suggest that efficiency of GaP solar cells could be strongly enhanced by means of the formation of an IB and encourage further research of supersaturated GaP with transition elements. **In particular, future research will be devoted to the confirmation of the existence of an intermediate band in GaP:Ti with alternative techniques.**

Acknowledgements

Authors would like to acknowledge C.A.I. de Técnicas Físicas of the Universidad Complutense de Madrid for ion implantation, rapid thermal annealing and Joule and e-beam evaporations, **and the technical and human support provided by Facility of Analysis and Characterization of Solids and Surfaces of SAIUEx (financed by UEX, Junta de Extremadura, MICINN, FEDER and FSE).** This work was partially supported by the Project MADRID-PV (Grant No. P2013/MAE-2780) funded by the Comunidad de Madrid, by the Spanish MINECO (Ministerio de Economía y Competitividad) under grants TEC 2013-41730-R and TEC 2015-69916-C2-1-R, and by the Universidad Complutense de Madrid (Programa de Financiación de Grupos de Investigación UCM–Banco Santander) under Grant 910173-2014. The work of D. Montero was supported by the Spanish MINECO under Contract BES-2014-067585. J. Solis from the Instituto de Optica is acknowledged for helpful discussions.

Supplementary information

Figure S1 shows the photogenerated voltage from the measurement of the spectral sheet photoconductance of a sample unimplanted and PLM processed and of a sample Ti implanted (8×10^{14} cm^{-2}) and PLM processed. The samples are the ones analyzed in Fig. 5.a of the main text. This supplementary information is added to avoid misinterpretations of results in Fig. 5.a, due to the similarity of the curves in the 550 – 650 nm range for these two samples. The measured voltage was extracted using the van der Pauw configuration and the lock-in amplifier as in Fig. 5.b. To calibrate this voltage to the sheet photoconductance magnitude shown in the main text, we measured the light power density outgoing the monochromator with a calibrated Si detector and used the method described in *J. Olea et al., J. Appl. Phys. 114, 053110 (2013)*. As it can be seen, the voltage at wavelengths over 550 nm are just noise for the unimplanted sample, and therefore no conclusions can be extracted in this range for this sample. For the sample Ti implanted the sheet photoconductance values are measurable up to around 850 nm.

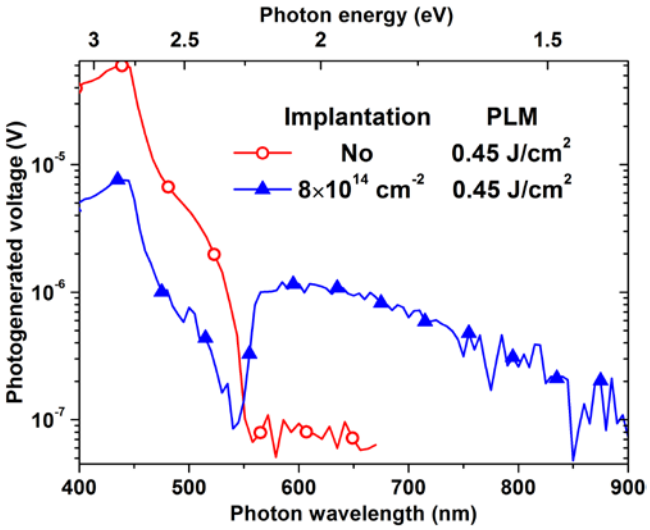

Figure S1. Photogenerated voltage from the measurement with the van der Pauw set up of the spectral sheet photoconductance of the sample unimplanted and PLM processed and the a sample Ti implanted (8×10^{14} cm^{-2}) and PLM processed, i.e. the same samples shown in Fig. 5.a.

Figure S2 shows the phase obtained by the lock-in amplifier in the measurement of the spectral sheet photoconductance shown in Fig. 5.a. There is a 40˚ abrupt increase at about 550 nm. This would mean different conduction mechanisms at energies above and below the GaP bandgap, supporting the hypothesis of conduction by different energy bands.

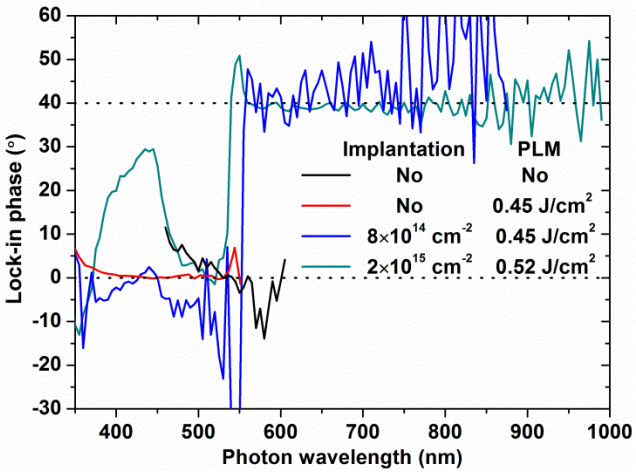

Figure S2. Phase obtained by the lock-in amplifier in the measurement of the spectral sheet photoconductance shown in Fig. 5.a.

Figure S3 shows the analysis for the rest of the samples shown in Fig. 5.a for the different transitions, following Eq. 1. The values extracted from this analysis are the ones shown in Table 1 of the main text.

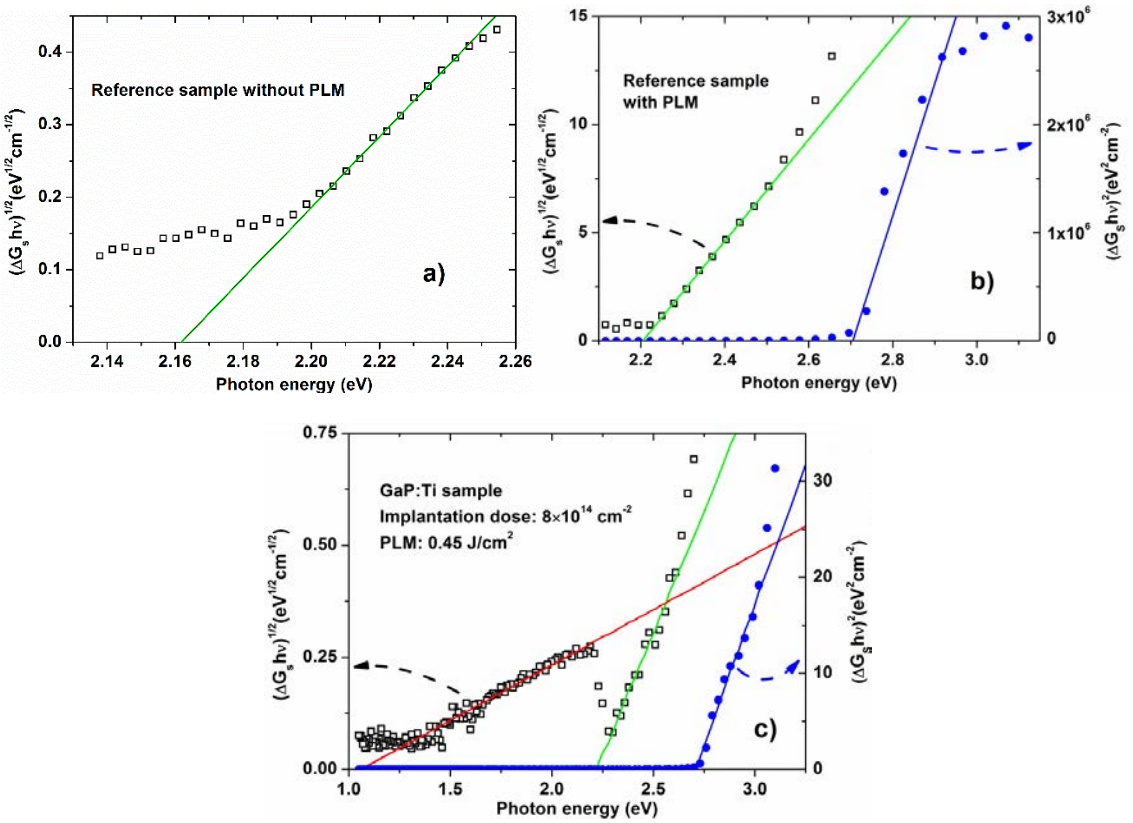

Figure S3. Fittings of the spectral sheet photoconductance data for the rest of the samples shown in Fig. 5.a to Eq. 1. The direct transition fittings corresponds to the right axis while the indirect transitions fittings correspond to the left axis.

References

[1] A. Luque, and A. Marti, "Increasing the efficiency of ideal solar cells by photon induced transitions at intermediate levels," *Physical Review Letters,* vol. 78, no. 26, pp. 5014-5017, Jun 30, 1997.

[2] A. Luque, A. Marti, and C. Stanley, "Understanding intermediate-band solar cells," *Nature Photonics,* vol. 6, no. 3, pp. 146-152, Mar, 2012.

[3] S. Ruhle, "Tabulated values of the Shockley-Queisser limit for single junction solar cells," *Solar Energy,* vol. 130, pp. 139-147, Jun, 2016.

[4] X. S. Lu, R. Y. Hao, M. Diaz, R. L. Opila, and A. Barnett, "Improving GaP Solar Cell Performance by Passivating the Surface Using AlxGa1-xP Epi-Layer," *Ieee Journal of the Electron Devices Society,* vol. 1, no. 5, pp. 111-116, May, 2013.

[5] C. R. Allen, J. M. Woodall, and J. H. Jeon, "Results of a gallium phosphide photovoltaic junction with an AR coating under concentration of natural sunlight," *Solar Energy Materials and Solar Cells,* vol. 95, no. 9, pp. 2655-2658, Sep, 2011.

[6] P. Wahnon, and C. Tablero, "Ab initio electronic structure calculations for metallic intermediate band formation in photovoltaic materials," *Physical Review B,* vol. 65, no. 16, Apr, 2002.

[7] C. Tablero, "Survey of intermediate band material candidates," *Solid State Communications,* vol. 133, no. 2, pp. 97-101, Jan, 2005.

[8] P. Palacios, J. J. Fernandez, K. Sanchez, J. C. Conesa, and P. Wahnon, "First-principles investigation of isolated band formation in half-metallic TixGa1-xP (x=0.3125-0.25)," *Physical Review B,* vol. 73, no. 8, Feb, 2006.

[9] C. Tablero, and P. Wahnon, "Analysis of metallic intermediate-band formation in photovoltaic materials," *Applied Physics Letters,* vol. 82, no. 1, pp. 151-153, Jan, 2003.

[10] S. Lauer, A. N. Danilewsky, J. Meinhardt, R. Hofmann, A. Dornen, and K. W. Benz, "Selected 3d-transition metals in gallium antimonide: Vanadium, titanium and iron," *Crystal Research and Technology,* vol. 32, no. 8, pp. 1095-1102, 1997.

[11] B. Clerjaud, "TRANSITION-METAL IMPURITIES IN III-V COMPOUNDS," *Journal of Physics C-Solid State Physics,* vol. 18, no. 19, pp. 3615-3661, 1985.

[12] J. J. Fernandez, C. Tablero, and P. Wahnon, "Application of the exact exchange potential method for half metallic intermediate band alloy semiconductor," *Journal of Chemical Physics,* vol. 120, no. 22, pp. 10780-10785, Jun, 2004.

[13] P. Palacios, P. Wahnon, S. Pizzinato, and J. C. Conesa, "Energetics of formation of TiGa3As4 and TiGa3P4 intermediate band materials," *Journal of Chemical Physics,* vol. 124, no. 1, Jan, 2006.

[14] C. Tablero, "Analysis of the optical properties for Ga4P3Ti compound with a metallic intermediate band," *Computational Materials Science,* vol. 36, no. 3, pp. 263-267, Jun, 2006.

[15] C. Tablero, "Optoelectronic properties analysis of Ti-substituted GaP," *Journal of Chemical Physics,* vol. 123, no. 18, Nov, 2005.

[16] A. Luque, A. Marti, E. Antolin, and C. Tablero, "Intermediate bands versus levels in non-radiative recombination," *Physica B-Condensed Matter,* vol. 382, no. 1-2, pp. 320-327, Jun 15, 2006.

[17] K. M. Yu, W. Walukiewicz, M. A. Scarpulla, O. D. Dubon, J. Wu, J. Jasinski, Z. Liliental-Weber, J. W. Beeman, M. R. Pillai, and M. J. Aziz, "Synthesis of GaNxAs1-x thin films by pulsed laser melting and rapid thermal annealing of N+-implanted GaAs," *Journal of Applied Physics,* vol. 94, no. 2, pp. 1043-1049, Jul, 2003.

[18] K. M. Yu, W. Walukiewicz, J. W. Ager, D. Bour, R. Farshchi, O. D. Dubon, S. X. Li, I. D. Sharp, and E. E. Haller, "Multiband GaNAsP quaternary alloys," *Applied Physics Letters,* vol. 88, no. 9, Feb, 2006.

[19] K. M. Yu, W. Walukiewicz, J. W. Beeman, M. A. Scarpulla, O. D. Dubon, M. R. Pillai, and M. J. Aziz, “Enhanced nitrogen incorporation by pulsed laser annealing of GaNxAs1-x formed by N ion implantation,” *Applied Physics Letters,* vol. 80, no. 21, pp. 3958-3960, May, 2002.

[20] W. C. W., and P. P. S., *Laser and electron beam processing of materials*, United Kingdom: Academic Press, Inc., 1980.

[21] D. Pastor, J. Olea, M. Toledano-Luque, I. Martil, G. Gonzalez-Diaz, J. Ibanez, R. Cusco, and L. Artus, “Laser thermal annealing effects on single crystal gallium phosphide,” *Journal of Applied Physics,* vol. 106, no. 5, Sep 1, 2009.

[22] D. Pastor, J. Olea, M. Toledano-Luque, I. Martil, G. Gonzalez-Diaz, J. Ibanez, R. Cusco, and L. Artus, “Pulsed Laser Melting Effects on Single Crystal Gallium Phosphide,” *Proceedings of the 2009 Spanish Conference on Electron Devices*, pp. 42-+, 2009.

[23] Y. Yuan, R. Hubner, F. Liu, M. Sawicki, O. Gordan, G. Salvan, D. R. T. Zahn, D. Banerjee, C. Baehtz, M. Helm, and S. Q. Zhou, “Ferromagnetic Mn-Implanted GaP: Microstructures vs Magnetic Properties,” *Acs Applied Materials & Interfaces,* vol. 8, no. 6, pp. 3912-3918, Feb, 2016.

[24] W. J. S., "Transient annealing of ion implanted Gallium Arsenide," *Mat. Res. Soc. Symp. Proc.,* 13, 1983].

[25] A. C. L., D. H. L., H. L. D., O. G. L., and V. K. V., "Annealing of implanted layers in compound semiconductors by localized beam heating techniques," *Laser and Electron Beam Processing of Materials*, 1980].

[26] R. T. Young, G. A. Vanderleeden, J. Narayan, W. H. Christie, R. F. Wood, D. E. Rothe, and J. I. Levatter, “CHARACTERIZATION OF EXCIMER LASER ANNEALING OF ION-IMPLANTED SI,” *Electron Device Letters,* vol. 3, no. 10, pp. 280-283, 1982.

[27] Z. Werner, M. Barlak, R. Ratajczak, P. Konarski, A. M. Markov, and R. Heller, “Electron-beam pulse annealed Ti-implanted GaP,” *Journal of Applied Physics,* vol. 120, no. 8, Aug, 2016.

[28] J. Solis, C. N. Afonso, and J. Piqueras, “EXCIMER LASER MELTING OF GAAS - REAL-TIME OPTICAL STUDY,” *Journal of Applied Physics,* vol. 71, no. 2, pp. 1032-1034, Jan, 1992.

[29] J. P. Mailoa, A. J. Akey, C. B. Simmons, D. Hutchinson, J. Mathews, J. T. Sullivan, D. Recht, M. T. Winkler, J. S. Williams, J. M. Warrender, P. D. Persans, M. J. Aziz, and T. Buonassisi, “Room-temperature sub-band gap optoelectronic response of hyperdoped silicon,” *Nature Communications,* vol. 5, Jan, 2014.

[30] W. Shan, W. Walukiewicz, J. W. Ager, E. E. Haller, J. F. Geisz, D. J. Friedman, J. M. Olson, and S. R. Kurtz, “Band anticrossing in GaInNAs alloys,” *Physical Review Letters,* vol. 82, no. 6, pp. 1221-1224, Feb, 1999.

[31] H. C. Casey, F. Ermanis, and K. B. Wolfstirn, “VARIATION OF ELECTRICAL PROPERTIES WITH ZN CONCENTRATION IN GAP,” *Journal of Applied Physics,* vol. 40, no. 7, pp. 2945-+, 1969.

[32] M. B. Panish, and H. C. Casey, “TEMPERATURE DEPENDENCE OF ENERGY GAP IN GAAS AND GAP,” *Journal of Applied Physics,* vol. 40, no. 1, pp. 163-&, 1969.

[33] T. Takizawa, “WAVELENGTH MODULATED REFLECTIVITIES OF THE DIRECT EXCITON EDGE IN GAP,” *Journal of the Physical Society of Japan,* vol. 52, no. 3, pp. 1057-1063, 1983.

[34] E. Garcia-Hemme, R. Garcia-Hernansanz, J. Olea, D. Pastor, A. del Prado, I. Martil, and G. Gonzalez-Diaz, “Meyer Neldel rule application to silicon supersaturated with transition metals,” *Journal of Physics D-Applied Physics,* vol. 48, no. 7, pp. 7, Feb, 2015.

[35] M. Miyao, K. Itoh, M. Tamura, H. Tamura, and T. Tokuyama, “FURNACE ANNEALING BEHAVIOR OF PHOSPHORUS IMPLANTED, LASER ANNEALED SILICON,” *Journal of Applied Physics,* vol. 51, no. 8, pp. 4139-4144, 1980.

[36] X. S. Lu, S. Huang, M. B. Diaz, N. Kotulak, R. Y. Hao, R. Opila, and A. Barnett, “Wide Band Gap Gallium Phosphide Solar Cells,” *Ieee Journal of Photovoltaics,* vol. 2, no. 2, pp. 214-220, Apr, 2012.

[37] R. F. Wood, and G. E. Giles, “MACROSCOPIC THEORY OF PULSED-LASER ANNEALING .1. THERMAL TRANSPORT AND MELTING,” *Physical Review B,* vol. 23, no. 6, pp. 2923-2942, 1981.

[38] T. A. Railkar, A. P. Malshe, W. D. Brown, S. S. Hullavarad, and S. V. Bhoraskar, “Ultrashort pulse ultraviolet laser treatment of n(100) GaAs: Microstructural modifications and passivation effects,” *Journal of Applied Physics,* vol. 89, no. 9, pp. 4766-4771, May, 2001.

[39] N. Yoshida, S. Chichibu, T. Akane, M. Totsuka, H. Uji, S. Matsumoto, and H. Higuchi, “SURFACE PASSIVATION OF GAAS USING ARF EXCIMER-LASER IN A H2S GAS AMBIENT,” *Applied Physics Letters,* vol. 63, no. 22, pp. 3035-3037, Nov, 1993.

[40] X. M. Ding, and J. J. Dubowski, "Stability of biofunctionalized GaAs surface - art. no. 64581C," *Proceedings of the Society of Photo-Optical Instrumentation Engineers (Spie).* pp. C4581-C4581, 2007.

[41] N. Lopez, L. A. Reichertz, K. M. Yu, K. Campman, and W. Walukiewicz, “Engineering the Electronic Band Structure for Multiband Solar Cells,” *Physical Review Letters,* vol. 106, no. 2, Jan, 2011.

[42] B. Marsen, S. Klemz, T. Unold, and H. W. Schock, “Investigation of the Sub-Bandgap Photoresponse in CuGaS2:Fe for Intermediate Band Solar Cells,” *Progress in Photovoltaics,* vol. 20, no. 6, pp. 625-629, Sep, 2012.

[43] Y. Berencen, S. Prucnal, F. Liu, I. Skorupa, R. Hubner, L. Rebohle, S. Zhou, H. Schneider, M. Helm, and W. Skorupa, “Room-temperature short-wavelength infrared Si photodetector,” *Scientific Reports,* vol. 7, pp. 9, Mar, 2017.

[44] E. Garcia-Hemme, R. Garcia-Hernansanz, J. Olea, D. Pastor, A. del Prado, I. Martil, and G. Gonzalez-Diaz, “Sub-bandgap spectral photo-response analysis of Ti supersaturated Si,” *Applied Physics Letters,* vol. 101, no. 19, Nov 5, 2012.

[45] T. S. Navruz, and M. Saritas, “Efficiency variation of the intermediate band solar cell due to the overlap between absorption coefficients,” *Solar Energy Materials and Solar Cells,* vol. 92, no. 3, pp. 273-282, Mar, 2008.